Journal of Cleaner Production 164 (2017) 1430–1445

Contents lists available at ScienceDirect

Journal of Cleaner Production

journal homepage: www.elsevier.com/locate/jclepro

Recovery of clean energy precursors from Bambara groundnut waste *via* pyrolysis: Kinetics, products distribution and optimisation using response surface methodology

Isah Yakub Mohammed [a, b, *], Yousif Abdalla Abakr [c], Jershen Nga Xing Hui [c], Peter Adeniyi Alaba [d], Kenobi Isima Morris [c], Mustapha Danladi Ibrahim [b]

[a] Department of Chemical and Environmental Engineering, The University of Nottingham Malaysia Campus, Jalan Broga, Semenyih, 43500, Selangor Darul Eshan, Malaysia
[b] Department of Chemical Engineering, Abubakar Tafawa Balewa University, P.M.B 0248, Bauchi, Nigeria
[c] Department of Mechanical, Manufacturing and Material Engineering, The University of Nottingham Malaysia Campus, Jalan Broga, Semenyih, 43500, Selangor Darul Eshan, Malaysia
[d] Department of Chemical Engineering, University of Malaya, Kuala Lumpur, 50603, Malaysia

ARTICLE INFO

Article history:
Received 9 January 2017
Received in revised form
6 July 2017
Accepted 8 July 2017
Available online 12 July 2017

Keywords:
Thermogravimetric analysis
Pyrolysis
Bambara groundnut shell
Energy analysis
Kinetic study

ABSTRACT

This study presents first comprehensive thermochemical analysis of Bambara groundnut shell. Pyrolysis characteristics was examined under non-isothermal degradation in nitrogen atmosphere at different heating rates (10, 15 and 20 °C/min) using single-step global model kinetic model. The single-step global model average apparent activation energy was found to be 142.64 ± 5.7 kJ/mol. Pyrolysis was conducted in a fixed bed reactor. Effects of pyrolysis temperature (450–750 °C), heating rate (20–50 °C/min) and nitrogen flow rate (5–25 L/min) were investigated collectively. The process variables were optimized using response surface methodology with central composite design. Optimum bio-oil yield of 36.49 wt% was recorded at 600 °C, 50 °C/min and 11 L/min. The bio-oil, bio-char and non-condensable gas collected were comprehensively characterised. Energy analysis of the products was also evaluated. This study revealed that Bambara groundnut shell, a residue from food crop, is a potential source of energy precursors for development of a sustainable bioenergy system and biomaterials.

1. Introduction

Fossil fuel is the major source of energy supply worldwide. According to the International Energy Outlook (IEO, 2016), fossil fuel will continue to be the dominant world energy source with about 78% contribution to total world energy use by end of 2040. Emission of greenhouse gases from the use of fossil fuel and the resulting environmental impact remains a global challenge. In November 2015, the United Nations conference on climate change held in Paris set a target to limit the global temperature rise to below 2 °C. Agricultural diversification was considered as parts of the measures towards achieving this goal in terms of developing opportunities for green energy and sustainable production systems. Currently, 75% of the world food is processed from rice, wheat, maize and soya beans. This raises another concern as these crops may not thrive in hotter climate to produce sufficient food for about 9 billion people in the near future as estimated by the United States Census Bureau, International Data Base (USCB, 2016).

Underutilised crops such as Bambara groundnut is one of the neglected crops with potential to grow under stressed environmental conditions. According to Mohale et al. (2014), Bambara groundnut is a drought tolerant crop and has high water use efficiency. The crop is predominantly cultivated by subsistence farmers throughout sub-Saharan Africa. Its grain is consumed as food and has superior dietary values. Brough and Azam-Ali (1992) reported that Bambara grain contains 16–25% protein, 42–60% carbohydrate and 5–6% lipid, which are important components of healthy diet for healthy human body development. These characteristics all together make Bambara groundnut to be increasingly popular and its cultivation currently spreading across Southeast Asia

* Corresponding author. Department of Chemical and Environmental Engineering, The University of Nottingham Malaysia Campus, Jalan Broga, Semenyih, 43500, Selangor Darul Eshan, Malaysia.
E-mail addresses: yimohd@atbu.edu.ng, kebx3iye@nottingham.edu.my (I.Y. Mohammed).

http://dx.doi.org/10.1016/j.jclepro.2017.07.068
0959-6526/

Abbreviations

CFF	Crops for the future
BGS	Bambara groundnut shell
TGA	Thermogravimetric analysis
DTG	Differential Thermogravimetric
SSGM	Single step global model
β	heating rate
ICTAC	International Confederation for Thermal Analysis and Calorimetry
OFW	Ozawa-Flynn-Wall
KAS	Kissinger–Akahira–Sunose
MKAS	Modified Kissinger–Akahira–Sunose
RSM	Response surface methodology
CCD	Central composite design
HHV	high heating value
TMS	Tamarind Shell
PNS	peanut shell
Eα	Activation Energy
ANOVA	analysis of variance
HC	hydrocarbons
PHOL	phenols
MEST	Methyl esters
AAK	Acids, aldehydes, and ketones
FTS	Fischer-Tropsch synthesis

(Mohammed et al., 2016a), suggesting that Bambara groundnut could be a major food security crop in the nearest future. Presently, Bambara groundnut is one of the crops being studied at the Crops for the Future (CFF) of the University of Nottingham Malaysia Campus, the first internal research organisation dedicated towards promoting and facilitating the use of neglected and underutilised crops.

Bambara groundnut shell (BGS) is the mass of pod wall after the grain has been removed. Studies have shown that the production of BGS can vary between 375 and 1000 kg/ha depending on the crop yield and landrace. Studies by Kishinevsky et al. (1996) on variation in nitrogen fixation and yield in landraces of Bambara groundnut reported BGS of 648–1107 kg/ha. Mwale et al. (2007) evaluated growth and development of Bambara groundnut in response to soil moisture reported an average of 596 kg/ha of BGS. Recent investigation by Musa et al. (2016) on effect of nitrogen fixation and N-balance of Bambara groundnut landraces grown on tropical acidic soils of Malaysia recorded 374–896 kg/ha of BGS. Despite the high yield of BGS, there is currently limited information on its valorisation into useful product or intermediate products.

Only recently, Mohammed et al. (2016a) reported first known study on valorisation of BGS into bio-oil via pyrolysis. The result presented by the authors revealed that BGS is a potential feedstock for high value biofuel precursor. However, the study was limited to classical investigation of pyrolysis temperature and other process variables such as nitrogen flow rate and heating rate were held constant. Studies on kinetics of thermal decomposition of BGS in an inert atmosphere has not been reported. Kinetic data from such examination will provides useful information about the decomposition profile and mechanisms, which is very important for the design of pyrolysis systems. In order to comprehensively evaluate the energy potential of the BGS, there is need to collectively examine the impact of the process variables on the product distribution. The objective of this study include thermogravimetric analysis of BGS and pyrolysis in a vertical fixed bed reactor. The study investigates effect of pyrolysis temperature, heating rate and nitrogen flow rate jointly on pyrolysis product distribution from BGS, optimization using response surface methodology and energy analysis.

2. Experimental

2.1. Materials and method

Bambara groundnut was locally grown at the crops for the future (CFF) field research centre (2°56′07.6″N 101°52′42.8″E) in Malaysia. After harvesting, shells from a landrace, EX-Sokoto BGS was collected and analysed. The material was oven dried at 105 °C and then shredded a rotor beater mill (SM100, Retsch GmbH, Germany) to particle sizes between 0.2 mm and 2.5 mm and stored in airtight plastic bags for further analysis. Proximate and ultimate analyses such as volatile matter, ash content, fixed carbon, elemental composition (Carbon, hydrogen, nitrogen, sulphur and oxygen), higher heating value and ash composition on a dry basis were determined according to standard analytical procedure detailed in Mohammed et al. (2016a). Thermogravimetric analysis (TGA) was conducted in nitrogen atmosphere (20 mL/min) with the aid of thermogravimetric simultaneous thermal analyser (STA) 6000 TGA (Perkin Elmer Sdn Bhd, Selangor, Malaysia), a powerful analytical technique for evaluating decomposition profile of solid samples. This technique allows acquisition of data relating the weight of sample and decomposition rate with respect to temperature, time or both under a controlled environment. The decomposition profile was evaluated from ambient temperature to 800 °C at three heating rates of 10, 15 and 20 °C/min. Sample size of approximately 10.0 mg (particle size of 0.2 mm) was used. The experiment was performed twice for reproducibility.

2.2. Kinetic modelling

2.2.1. Single-step global model (SSGM)

The kinetic analysis of the samples was examined by single step global model (SSGM) to evaluate the kinetic triplets such as pre-exponential factor, activation energy, and mechanism model. The SSGM is the simplest kinetics model which assumes that the decomposition rate of the pyrolysis process depends on an arbitrary reaction order according to reaction scheme represented in Eq. (1). Generally, the rate of reaction for heterogeneous material in a TGA process is given by Eq. (2).

$$Biomass \xrightarrow{k} Volatile + char \tag{1}$$

$$\frac{d\alpha}{dT} = k(T)f(\alpha) \tag{2}$$

k(T) is the temperature dependent constant of the reaction; $f(\alpha)$ is the reaction mechanism model for an ideal reaction. T is the absolute temperature in Kelvin and α is the conversion, which is given by:

$$\alpha = \frac{m_0 - m_t}{m_0 - m_f} \tag{3}$$

m_0 is the initial sample mass; m_t is the sample mass at a specific

time; m_f is the post-pyrolysis sample mass. By applying the Arrhenius law, the term k(T) in Eq. (2) becomes:

$$k(T) = Aexp\left(-\frac{E}{RT}\right) \quad (4)$$

where R is the ideal gas constant, which is 8.314 J mol^{-1} K^{-1}; A is the apparent pre-exponential factor in min^{-1} and E is the activation energy in J mol^{-1}. By applying linear non-isothermal TG heating rate ($\beta = dT/dt$) and combining Eq. (4), Eq. (2) turned to:

$$\frac{d\alpha}{dT} = \frac{A}{\beta}exp\left(-\frac{E}{RT}\right)f(\alpha) \quad (5)$$

2.2.2. Computation of activation energy

Several model-free methods have applied Eq. (5) to estimate the kinetic parameters using multiple β for the TG experiments. For a one-step decomposition process, model-free techniques like Ozawa-Flynn-Wall (OFW), Starink, Friedman and Kissinger–Akahira–Sunose (KAS) are used to evaluates E at various α without assumption of any specific reaction model. Therefore, based on the ICTAC Kinetics Committee recommendations (Vyazovkin et al., 2011), an accurate estimation of E_α could be achieved from a modified Kissinger–Akahira–Sunose (MKAS) method formulated using Starink equation as expressed in Eq. (6).

$$ln\frac{\beta_i}{T_{\alpha,i}^{1.92}} = Const - 1.0008\left(\frac{E_\alpha}{RT_\alpha}\right) \quad (6)$$

T_α and E_α are the temperature and apparent activation energy at a specific α, respectively. This study used MKAS method to determine the value of E_α for the pyrolysis of SKT. The value of E_α is evaluated from the slope of the linear graph of $ln\frac{\beta_i}{T_{\alpha,i}^{1.92}}$ versus $1/T_\alpha$.

2.2.3. Reaction mechanism model

To evaluate reaction kinetic model f(α), some mathematical models that describes the solid-state reaction kinetics are employed as summarised in Table 1. According to master-plots method (Starink, 2003), y(α) function is given in Eq. (7) and was adopted in this study.

$$y(\alpha) = \left(\frac{d\alpha}{dT}\right)_\alpha exp\left(\frac{E_0}{RT_\alpha}\right) = Af(\alpha) \quad (7)$$

E_0 (J/mol) is the average value of E_α computed by MKAS method; $(d\alpha/dT)_\alpha$ is the derivative of conversion with respect to temperature at a specified α and a particular β. The experimental master plots are obtained from the plot of y(α) versus α. The theoretical master plots models (Table 1) is determined by substituting the same α into the kinetic models and plotting f(α) vs. α. Since the value of A in Eq. (7) is not yet known, the experimental and theoretical y(α) plots could be normalized (Eq. (8)) between 0 and 1. The most appropriate mechanistic model is obtained by matching the experimental and theoretical $y(\alpha)_{norm}$.

$$y(\alpha)_{norm} = \frac{y(\alpha)}{\max[y(\alpha)]} \quad (8)$$

2.2.4. Computation of pre-exponential factor

Having identified the suitable model f(α), Eq. (5) can be used to compute the best suitable A_α as presented in Eq. (9)

$$f(\alpha) = \beta\left(\frac{d\alpha}{dT}\right)_\alpha\left[A_\alpha exp\left(\frac{E_0}{RT_\alpha}\right)\right]^{-1} \quad (9)$$

A_α is the pre-exponential factor at a specific conversion. However, in SSGM, estimation of pre-exponential factor (A_0) is not possible by determination of the average of A_α because of "compensation effect (CE)", and the variation between E_α and A_α. Lesnikovich and Levchik (1983) stated that the invariant kinetic method that uses CE to establish a strong correlation between E_α and A_α is called CE equation and is given by Eq. (10).

$$lnA_\alpha = a^*E_\alpha + b^* \quad (10)$$

where a^* and b^* are constants and is determined from the slope and intercept of the linear plot of lnA_α versus E_α, respectively. Then the value of A_0 can be computed by substituting the obtained values of a^* and b^* back into Eq. (10).

2.3. Pyrolysis and products characterisation

Pyrolysis is the thermal decomposition of biomass under inert atmosphere to produce liquid (bio-oil), solid (bio-char), and gas (non-condensable) products. This technique remains attractive as it consists of fewer steps and can process any biomass material. In this study, intermediate pyrolysis was employed in order produce less reactive tar that can be directly applied as fuel in boilers and engines in addition to dry bio-char suitable for both agricultural and energy applications. The pyrolysis system consists of a stainless steel vertical fixed bed reactor (5 cm in diameter, and length 115 cm) with a distribution plate (hole diameter of 1.0 mm) placed inside it at 25 cm from the bottom (Fig. 1). For each run, 200 g of BGS (bone dry, approximately 2.5 mm particle size) was placed on the distribution plate inside the reactor and the system was heated electrically. A k-type thermocouple connected to a computer through data logger was used to constantly monitor the reaction temperature inside the reactor. The pyrolysis vapour was condensed by passing through a condenser connected to a chiller operating at 3 °C with water as coolant and the oil was collected and weighed before further analysis. The bio-char was collected after the reactor had cooled down to room temperature. The bio-oil, bio-char and non-condensable gas yield was computed according to equations (11)–(13). Design of experiment was carried out using response surface methodology (RSM) approach with central composite design (CCD). This technique gives reliable measurements of a response or responses, which may be influenced by many process variables. Twenty (20) sets of experimental conditions were generated using design expert software (Version 6.0.6, Stat-Ease Inc., MN, USA) with pyrolysis temperature (450–750 °C), nitrogen flow rate (5–20 L/min) and heating rate (20–50 °C/min) as the process variables.

$$Bio-oil\ yield\ (wt\ \%) = \left(\frac{weight\ of\ bio-oil\ collected}{weight\ of\ biomass\ feed}\right) \times 100 \quad (11)$$

$$Bio-char\ yield\ (wt\ \%) = \left(\frac{weight\ of\ bio-char\ collected}{weight\ of\ biomass\ feed}\right) \times 100 \quad (12)$$

$$Non-condensable\ yield\ (wt\ \%) = [100 - Eq.(11) + Eq(12)] \quad (13)$$

Table 1
Mathematical expression of an ideal reaction model in solid-state SSGM (Vyazovkin et al., 2011).

Models	Description	$f(\alpha)$
Reaction order	First-order (L1)	$1 - \alpha$
	Second-order (L2)	$(1 - \alpha)^2$
	Third-order (L3)	$(1 - \alpha)^3$
Diffusion	1-D diffusion (D1)	$1/2\alpha$
	2-D diffusion (D2)	$[-\ln(1 - \alpha)]^{-1}$
	3-D diffusion-Jander (D3)	$[3/2(1 - \alpha)^{2/3}]/[1-(1 - \alpha)^{1/3}]$
	Ginstling-Brounshtein (D4)	$[3/2(1 - \alpha)^{1/3}]/[1-(1 - \alpha)^{1/3}]$
Nucleation	Avrami-Erofeyev (A1)	$2(1 - \alpha)[-\ln(1 - \alpha)]^{1/2}$
	Avrami-Erofeyev (A2)	$3(1 - \alpha)[-\ln(1 - \alpha)]^{1/3}$
	Avrami-Erofeyev (A3)	$1.5(1 - \alpha)[-\ln(1 - \alpha)]^{1/3}$
	Avrami-Erofeyev (A4)	$4(1 - \alpha)[-\ln(1 - \alpha)]^{3/4}$
Geometrical contraction	Contracting area (R2)	$2(1 - \alpha)^{1/2}$
	Contracting volume (R3)	$3(1 - \alpha)^{1/3}$
Power law	2/3-Power law (P2/3)	$(2/3)\alpha^{-1/2}$
	2-Power law (P2)	$2\alpha^{1/2}$
	3-Power law (P3)	$3\alpha^{1/3}$
	4-Power law (P4)	$4\alpha^{1/4}$

Physicochemical characteristics of bio-oil such as pH, density, high heating value (HHV) and water content of bio-oil were determined following standard analytical procedures outlined in Mohammed et al. (2016a, 2017). Bio-oil chemical composition was determined with the aid of gas chromatograph-mass spectrometer, GC-MS (PerkinElmer Clarus®SQ8 Akron, OH, USA). Bio-char properties were analyses following the same analytical procedure adopted for the proximate and ultimate characterization of the feedstock. Scanning electron microscopy, SEM-EDX (FEI Quanta 400 FE-SEM, Hillsoboro, OR, USA) was used to evaluate the surface characteristics of bio-char and ASAP 2020 physisorption analyser (Micrometrics, USA) was used to determine the specific surface area and pore properties of bio-char.

3. Results and discussion

3.1. Feedstock characteristics

Summary of result of physicochemical properties of BGS is given in Table 2. On dry basis, the BGS has high volatile matter of 73.83 wt %, ash content of 10.10 wt%. The result of elemental composition (CHNSO) revealed the BGS is made up of carbon (C: 34.63 wt%), hydrogen (H: 11.28 wt%), nitrogen (N: 1.16 wt%), sulphur (S: 1.0 wt %) and oxygen (O: 51.93 wt%). Calorific value (higher heating value-HHV) determined using oxygen bomb calorimeter was 19.19 MJ/kg. In comparison with other biomass such as Tamarind Shell (TMS) and peanut shell (PNS), the BGS volatile matter is about 10.52–12.89% (Table 2) higher compared to the volatile matter of TMS and PNS as reported by Kuprianov and Arromdee (2013), which could also be responsible for the HHV recorded in the BGS (19.19 MJ/kg) relative to about 16.0 MJ/kg reported for TMS and PNS. The major inorganic component in the BGS was potassium (K) relative to TMS and PNS, which constituted predominantly calcium (Ca) and silica (Si) respectively. This dissimilarity in the minerals is due to the fact that the shells are of different origin. In addition, it could also be as a result of differences in pre-characterisation handling as inorganic material are said to be incorporated in the biomass during the fuel handling stage (Mohammed et al., 2016b).

The TG/DTG profile BGS at different heating rates in inert atmosphere is shown Fig. 2. Pyrolysis characteristics of the sample displayed three distinct regions. Stage I occurred at temperature below 200 °C for all the heating rates (10, 15 and 20 °C/min) investigated in this study, which is associated to dehydration of moisture and release of low volatile matters. The corresponding weight loss of recorded was between 0.92 and 2.14 wt%. Stage II represent the active pyrolysis state with temperature between 200 and 400 °C. This stage is characterised by a visible shoulder and maximum degradation peak, which are ascribed to thermal decomposition of hemicellulose and cellulose with an average total weight loss of 50.89 wt%. Stage III can be regarded as passive pyrolysis stage at temperature above 400 °C. The degradation profile of the sample shows a continuous gradual weight loss, which can be related lignin decomposition. The average weight loss recorded under this region is about 17.37 wt%. Summary of weight loss and temperature regime at different heating is presented in Table 3. The pyrolysis profile exhibited by the BGS is similar to degradation profile of other lignocellulosic biomass. Studies reported by Mohammed et al. (2015a,b) and Yakub et al. (2015) on characterization of Napier grass and oil palm residues revealed that thermal degradation profiles are characterised by shoulders and peaks at various temperatures. The authors observed shoulders at around 200 and 270 °C on the DTG pattern of Napier grass, which was ascribed to thermal decomposition of extractives and hemicellulose respectively. Maximum decomposition Napier grass was observed at about 320 °C and attributed to cellulose degradation. A gradual decomposition of lignin was also observed at temperature above 400 °C. Oil palm fronds and oil palm trunk exhibited similar thermogravimetric characteristics within the same temperature regimes. Pyrolysis characteristics of woody biomass reported by Biswas et al. (2011) displayed comparable degradation profile.

3.2. Single-step global model kinetic analysis

The DTG profiles of the BGS recorded at different heating rates (β: 10, 15 and 20 °C) were used with MKAS methods to determine the kinetic triplet. Fig. 3 shows plot of ln ($\beta/T^{1.92}$) versus 1/T and the value of E_α was estimated from the slope at certain conversion (α). The α-value in the range of 0.05–0.95 with a step size of 0.05 was used to estimate apparent E_α. Fig. 4 illustrates the relationship between E_α and α and its accuracy using the linear R^2 value. The E_α increased with increasing α-value up to 0.58 and thereafter decreased from 0.58 to 0.72 (Fig. 4a). The value of E_α changed to negative from α-value of 0.674, which is attributed to the less devolatilization rate and continuous change in the pyrolysis mechanisms, suggesting some multicomponent complex reactions. The increased conversion recorded under this region is attributed to both multicomponent decomposition of residual solid and secondary reaction propagated by the increase in temperature and catalytic effects of inorganic minerals present in the source biomass. This observation is similar to the pyrolysis characteristics

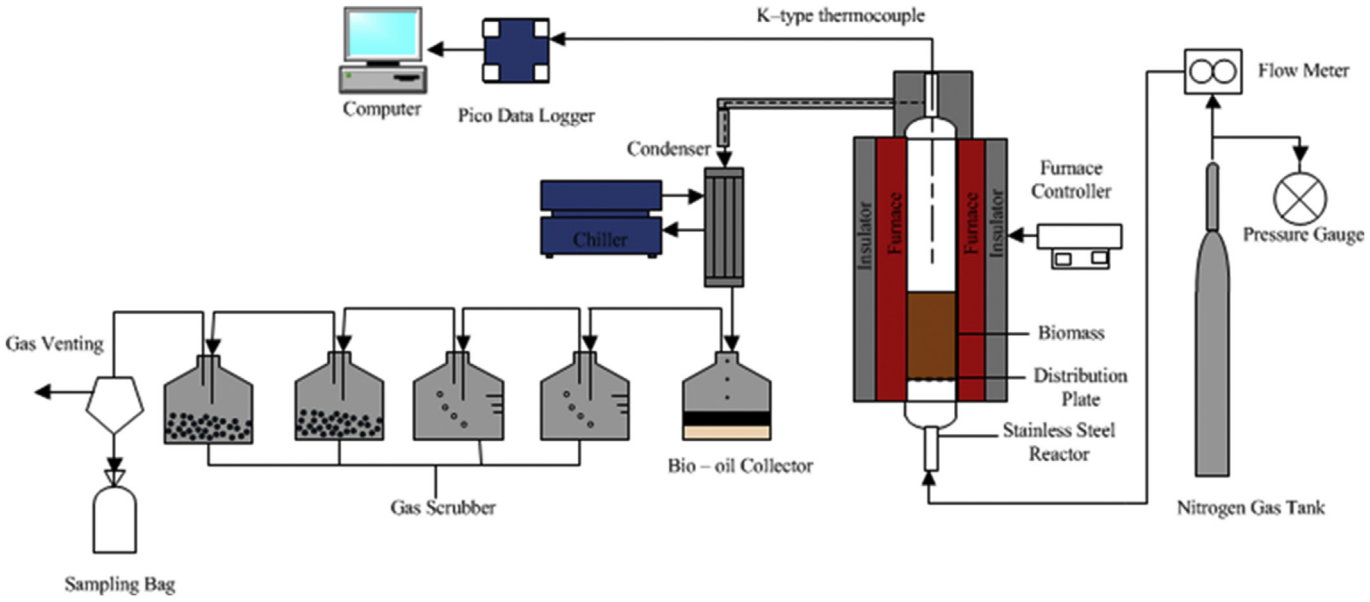

Fig. 1. Pyrolysis Experimental setup.

Table 2
Characteristics of BGS feedstock.

Property	BGS	PNS	TMS
Proximate analysis (wt% dry basis)			
VM (wt %)	73.83 ± 1.39	65.40	66.8
AC (wt %)	10.10 ± 0.41	5.70	2.90
FC (wt %)[a]	16.08 ± 0.71	19.60	21.70
HHV (MJ/kg)	19.19 ± 0.01	16.40	16.30
Ultimate analysis (wt% dry basis)			
C	34.63 ± 0.92	56.59	53.90
H	11.28 ± 0.22	6.45	5.92
N	1.16 ± 0.04	1.53	0.63
S	1.00 ± 0.01	0.09	0.02
O[b]	51.93 ± 1.16	35.34	39.53
Mineral composition (EDX)			
Magnesium (Mg)	2.57 ± 0.07	1.96	3.02
Aluminium (Al)	4.15 ± 0.11	11.60	0.63
Silica (Si)	5.01 ± 0.14	18.24	0.22
Phosphorous (P)	3.84 ± 0.10	0.95	1.51
Sulphur (S)	4.59 ± 0.12	1.02	0.43
Chlorine (Cl)	7.27 ± 0.20	–	–
Potassium (K)	72.57 ± 2.10	9.34	18.99
Calcium (Ca)	nd	4.43	46.54
Iron (Fe)	nd	8.11	0.17

VM: volatile matter; AC: ash content; FC: fixed carbon; HHV: higher heating value; C: carbon; H: hydrogen; N: nitrogen; S: sulphur; O: oxygen.
[a] By difference [100-(AC + VM)].
[b] [O = 100-(C + H + N + S)]; Values are the means (n = 3) ± standard deviation. (SKT-BGS) Ex-Sokoto Bambara groundnut shell; (PNS) Peanut shell and (TMS) Tamarind Shell.

of corn stover and cocoa shell biomass reported by Patnaik and Goldfarb (2015). They recorded negative activation energies, which were attributed to decreased devolatilization rate as a result of mass transport of gases from the sample surface. The composition of evolved gases detected under the negative apparent activation energies were mainly methane and acetylene, which are generally products of secondary reaction and further aromatization of residual solid (Collard and Blin, 2014). In this study, the average value of apparent E_α recorded for the BGS is 142.64 ± 5.7 kJ/mol. Consequently, the MKAS method employed adequately modelled the pyrolysis kinetic behaviour of BGS. This is also evident in the R^2 versus conversion plot (Fig. 4b). The R^2-values are coefficient of regression obtained from the MKAS plot (Fig. 3). The R^2-values at conversions between 0.3 and 0.7 tends to unity, which connote perfect fit. This trend is in consonant with our earlier observation as this region represents the active pyrolysis of the BGS. The $y(\alpha)$

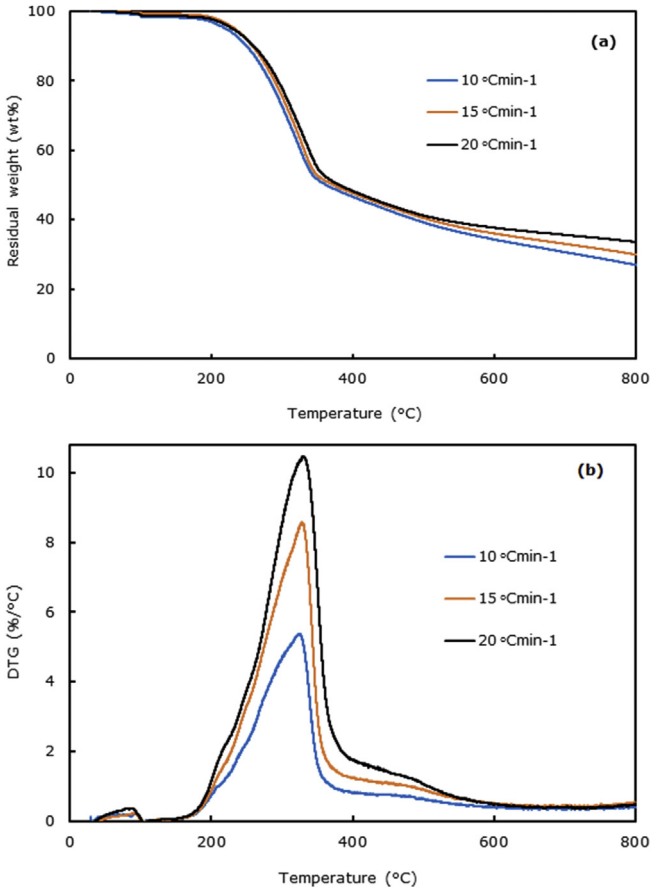

Fig. 2. Thermogravimetric profile of SKT-BGS at different heating rates (a) TG curve (b) DTG curve.

master plot and the CE plot are shown in Fig. 5. The decomposition kinetics of BGS followed theoretical diffusional model, precisely the D3 model (Fig. 5a). This implies that to a large extent, SSGM is suitable for modelling the BGS. The pre-exponential factor was estimated using the Eq. (9). The values of $f(\alpha)$ was obtained from the D3 model (Table 1). Fig. 5b shows the linear plots of $\ln A_\alpha$ versus E_α. The corresponding A_α, SSGM kinetic model, CE model and pre-exponential factor (A_0) were computed accordingly and summarized in Table 4.

3.3. Central composite design (CCD) and statistical analysis

Pyrolysis experiments were conducted according to the experimental designed matrix and the responses (pyrolysis products) are presented in Table 5. Experimental data were fitted quadratic model in terms of code factors as shown in the (14), (15) and (16) below, with A, B and C representing the temperature (°C), nitrogen flow rate (L/min) and heating rate (°C/min). Each model was tested for analysis of variance (ANOVA) to establish its significance and nature of interactions between the process variables.

$$\begin{aligned} Bio-oil\ (wt\ \%) = 31.31 &+ 1.39\ (A) + 0.51\ (B) \\ &- 2.71(C) - 2.05\left(A^2\right) \\ &+ 3.01\left(B^2\right) - 3.50\left(C^2\right) - 0.15\ (AB) \\ &+ 2.45\ (AC) + 1.02\ (BC) \end{aligned} \quad (14)$$

$$\begin{aligned} Bio-char\ (wt\ \%) = 37.23 &- 6.46\ (A) - 0.42(B) + 2.64\ (C) \\ &+ 2.46\left(A^2\right) + 0.52\left(B^2\right) - 1.39\left(C^2\right) \\ &+ 0.40(AB) - 3.90\ (AC) - 0.67(BC) \end{aligned} \quad (15)$$

$$\begin{aligned} Non-condensable\ gas\ (wt\ \%) = 31.46 &+ 5.08\ (A) - 0.089(B) \\ &+ 0.073\ (C) - 0.41\left(A^2\right) \\ &- 3.53\left(B^2\right) + 4.90\left(C^2\right) \\ &- 0.25\ (AB) \\ &+ 1.45\ (AC) - 0.35(BC) \end{aligned} \quad (16)$$

The results of analysis of variance (ANOVA) for bio-oil yield, bio-char yield and non-condensable gas yield are summarised in Table 6(a-c). The results showed that factor A, C, A^2, B^2, C^2, AC and BC are the significant model terms for bio-oil yield, having the value of "Prob > F" less than 0.005. The analysis also reveal that A, C, A^2, AC and A, B^2, C^2, AC represent significant model terms for bio-char and non-condensable gas yield respectively. The "Lack of Fit F-value" recorded for all the responses were not significant relative to the pure error. The predicted responses by software using the quadratic models are reasonably close to the experimental values recorded, having R-square value of more than 0.900 (bio-oil: 0.9716, bio-char: 0.9702 and non-condensable gas: 0.9505).

Table 3
Thermal degradation characteristics of BGS at different heating rates.

Stage	Heating rate (°C/min)	T_i (°C)	T_f (°C)	WL (%)
I	10	~	179.53	2.14
	15	~	167.54	0.92
	20	~	187.12	1.78
II	10	179.53	400.00	51.24
	15	167.54	400.00	51.46
	20	187.12	400.00	49.98
III	10	400.00	800.00	19.70
	15	400.00	800.02	17.68
	20	400.00	799.86	14.66
Residue (wt %)	10		26.92	
	15		29.94	
	20		33.57	

"~" is ambient temperature; (T_i), (T_f) is the initial temperature and final temperature; (WL) weight loss.

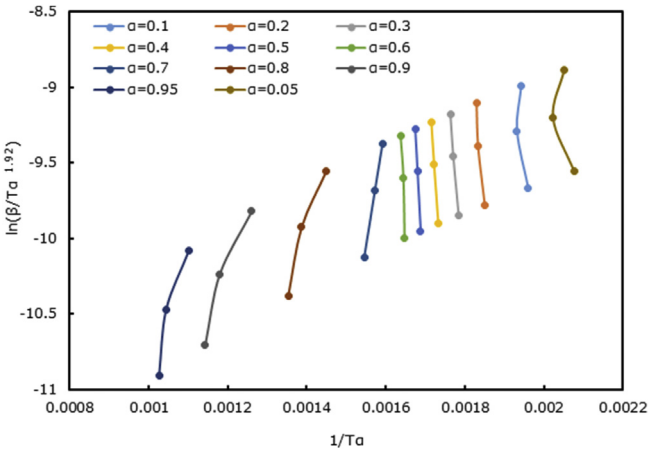

Fig. 3. SKT-BGS MKAS linear plots.

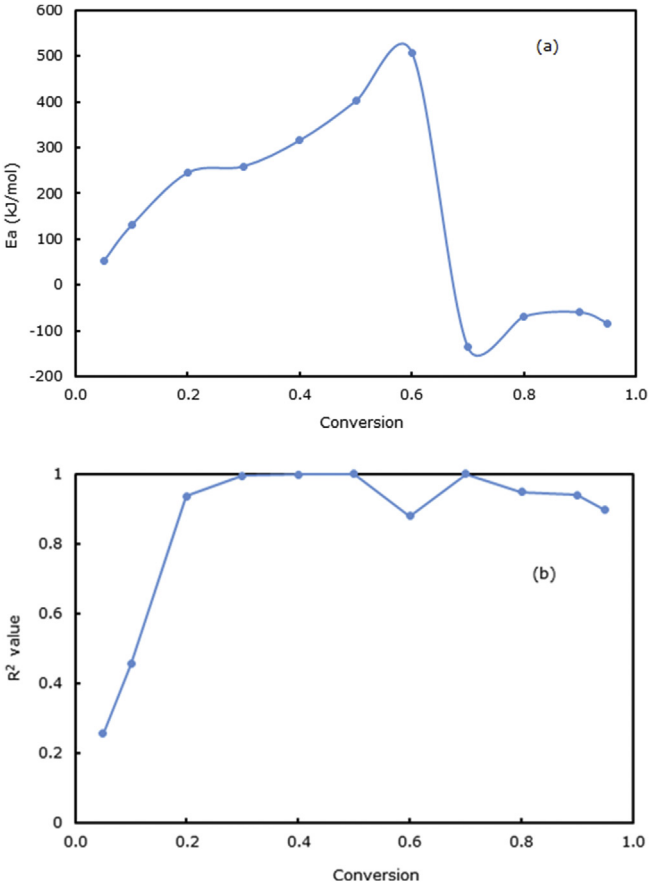

Fig. 4. BGS pyrolysis kinetic parameters estimation by MKAS method. (a) change in activation energy (b) R^2 value with conversion.

Similarly, the "Pred R-squared" values were in reasonable agreement with "Adj R-squared". From the diagnostics shown in Fig. 6, all the data were evenly distributed about a best straight line of fit, indicating homoscedasticity and suitability of the models.

3.4. Effect of process variables on the yield of bio-oil, bio-char and non-condensable gas

Figure 7 shows 3D response surface and interaction plots between the process variable for bio-oil yield. Increasing heating rate from 20 °C/min to 50 °C/min led to increase in the bio-oil yield (Fig. 7a) under constant nitrogen flow of 12.5 L/min. At 450 °C, the oil yield recorded was 30.22 wt% at 20 °C/min compared 50 °C/min heating rate, which produced 31.54 wt% at under the same temperature. As the temperature increased to 600 °C, the bio-oil yield recorded was 32.93 and 35.69 wt% at 20 °C/min and 50 °C/min respectively. The increased bio-oil yield recorded with temperature at higher heating rate (50 °C/min) is due to rapid devolatilization of biomass and thermal degradation of high molecular weight organic structures within the char and subsequently results in the bio-oil yield (Imam and Capareda, 2012; Mohammed et al., 2017). The maximum bio-oil yield recorded was 35.0 wt% at 600 °C, 12.5 L/min and 50 °C/min, which is approximately 9% higher than the bio-oil yield recorded from the classical pyrolysis studies of SKT-BGS reported by Mohammed et al. (2016a) at similar pyrolysis temperature and heating rate. As the temperature increased beyond 600 °C, the pyrolysis oil yield decreased due to formation of more non-condensable gas by rigorous cracking of high molecular weight volatiles at high temperature (Imam and Capareda, 2012).

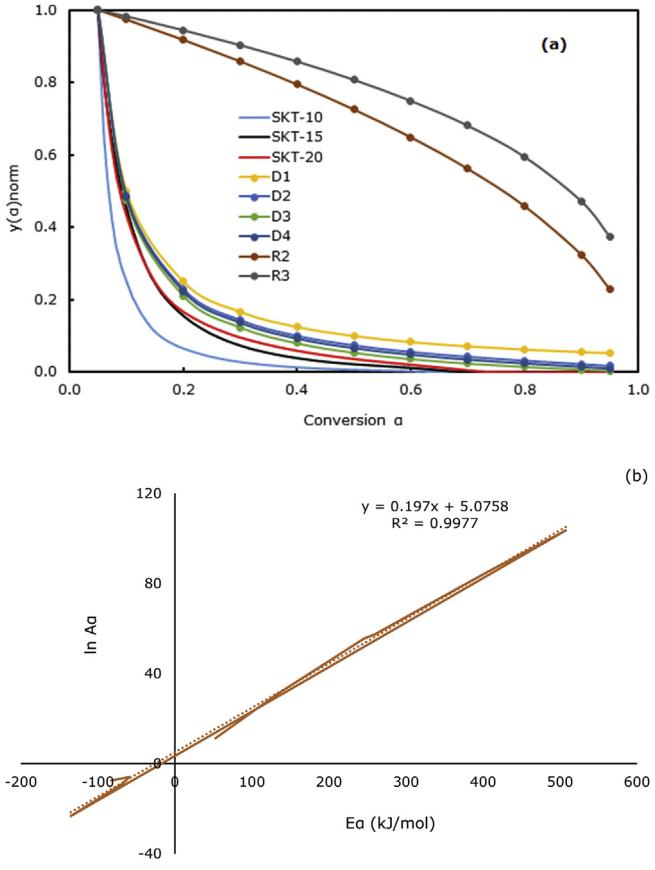

Fig. 5. (a) Experimental and several theoretical normalized y(α) plot versus conversion (α); (b) Compensation Effect.

Table 4
Characteristics of apparent activation energy and pre-exponential factor calculated from D3 model.

β (°C/min)	A_{min} (min^{-1})	A_{max} (min^{-1})
10	7.81E−11	9.25E+44
15	2.21E−10	3.31E+45
20	8.66E−10	4.78E+45

CE equation	Ao_{min}	SSGM kinetic equation
$\ln A_\alpha = 0.197 \times 10^{-3} \times E_\alpha + 5.08$	2.56×10^{14}	$\frac{d\alpha}{dT} = \frac{3.84 \times 10^{14}}{\beta} \exp\left(-\frac{17156.6}{T}\right) \times (1-\alpha)^{2/3}[1-(1-\alpha)^{1/3}]^{-1}$

Interaction between pyrolysis temperature and nitrogen flow rate at constant heating rate (35 °C/min) is presented in Fig. 7b. Increasing pyrolysis temperature from 450 to 600 °C increased bio-oil yield at both 5 L/min and 20 L/min nitrogen flow regimes, though at different proportions. Bio-oil collected under 5 L/min was 54% higher compared to the bio-oil recorded under 20 L/min nitrogen flow at the same temperature (450 °C). Higher bio-oil yield under 5 L/min was recorded up to 600 °C relative to 20 L/min but thereafter attained the same value at 750 °C. This trend observed under 5 L/min clearly elucidates that secondary cracking of pyrolysis vapour is more severe with increasing temperature and significantly decreased bio-oil yield. On the other hand, the increasing pattern in bio-oil yield recorded with increasing temperature under 20 L/min nitrogen flow indicates that fast evacuation of volatiles increased bio-oil despite increase in the pyrolysis temperature. The lower bio-oil recorded under 20 L/min at temperatures below 750 °C is due to short residence time of condensing volatiles in the condenser and thereby some escaping as parts of the non-condensable gas (Muradov et al., 2012). Fig. 7c shows impact of heating rate and nitrogen flow rate on bio-oil yield under a constant pyrolysis temperature (600 °C). It can be observed that more bio-oil yield was recorded under 5 L/min compared to 20 L/min throughout the investigated heating rates (20–50 °C/min). However, below 35 °C/min, no significant change in bio-oil yield was recorded at 20 L/min. The difference in the oil yield was within 5.0% compare to 12.0% recorded at 5 L/min under the same heating rate conditions. With increasing heating rate beyond

Table 5
Central composite experimental design matrix and responses.

Standard run	A	B	C	Responses (wt %)		N/gas
	(°C)	(°C/min)	(L/min)	Bio-char	Bio-oil	
20	600	35	12.5	38.47	31.43	30.10
13	600	35	5.0	32.53	30.39	37.08
17	600	35	12.5	36.47	31.93	31.60
7	450	50	20.0	50.49	24.20	25.31
19	600	35	12.5	38.50	30.40	31.10
4	750	50	5.0	34.65	29.65	35.70
16	600	35	12.5	38.00	30.90	31.10
15	600	35	12.5	37.47	31.43	31.10
12	600	50	12.5	35.89	35.69	28.42
3	450	50	5.0	38.69	31.89	29.41
11	600	20	12.5	37.29	32.93	29.78
18	600	35	12.5	39.11	31.79	29.10
9	450	35	12.5	45.92	26.95	27.13
10	750	35	12.5	31.14	31.55	37.31
2	750	20	5.0	33.38	30.78	35.84
5	450	20	20.0	53.53	20.62	25.85
8	750	50	20.0	31.21	30.47	38.32
6	750	20	20.0	32.25	28.80	38.96
14	600	35	20.0	36.82	25.22	37.97
1	450	20	5.0	38.66	33.71	27.64

Responses are the average values (n = 2). N/gas: non-condensable gas.

Table 6
ANOVA test for response models and respective model term (a): bio-oil; (b): bio-char (c): non-condensable gas.

Source	Sum of Squares	DF	Mean Square	F-Value	Prob > F	Remark
(a)						
Model	222.44	9	24.72	38.03	<0.0001	significant
A	19.22	1	19.22	29.58	0.0003	significant
B	2.56	1	2.56	3.93	0.0755	
C	73.51	1	73.51	113.12	<0.0001	significant
A^2	11.59	1	11.59	17.84	0.0018	significant
B^2	24.84	1	24.84	38.23	0.0001	significant
C^2	33.71	1	33.71	51.87	<0.0001	significant
AB	0.19	1	0.19	0.29	0.6013	
AC	48.06	1	48.06	73.96	<0.0001	significant
BC	8.40	1	8.40	12.93	0.0049	significant
Residual	6.50	10	0.65			
Lack of Fit	4.86	5	0.97	2.96	0.1295	not significant
Pure Error	1.64	5	0.33			
Cor Total	228.93	19				
Std. Dev.	0.8061		R-Squared	0.9716		
Mean	30.0367		Adj R-Squared	0.9461		
C.V.	2.6837		Pred R-Squared	0.7694		
PRESS	52.7861		Adeq Precision	25.0745		
(b)						
Model	640.20	9	71.13	36.14	<0.0001	significant
A	417.89	1	417.89	212.29	<0.0001	significant
B	1.74	1	1.74	0.88	0.3696	
C	69.58	1	69.58	35.35	0.0001	significant
A^2	16.64	1	16.64	8.45	0.0156	significant
B^2	0.75	1	0.75	0.38	0.5506	
C^2	5.35	1	5.35	2.72	0.1303	
AB	1.31	1	1.31	0.67	0.4336	
AC	121.97	1	121.97	61.96	<0.0001	significant
BC	3.63	1	3.63	1.84	0.2046	
Residual	19.68	10	1.97			
Lack of Fit	15.35	5	3.07	3.54	0.0959	not significant
Pure Error	4.34	5	0.87			
Cor Total	659.89	19				
Std. Dev.	1.403		R-Squared	0.9702		
Mean	38.0236		Adj R-Squared	0.9433		
C.V.	3.6898		Pred R-Squared	0.8763		
PRESS	81.6239		Adeq Precision	23.101		
(c)						
Model	352.32	9	39.15	21.35	<0.0001	significant
A	257.86	1	257.86	140.62	<0.0001	significant
B	0.08	1	0.08	0.04	0.84	
C	0.05	1	0.05	0.03	0.8672	
A^2	0.45	1	0.45	0.25	0.6292	
B^2	34.24	1	34.24	18.67	0.0015	significant
C^2	65.91	1	65.91	35.94	0.0001	significant
AB	0.50	1	0.50	0.27	0.6116	
AC	16.90	1	16.90	9.22	0.0126	significant
BC	0.99	1	0.99	0.54	0.4794	
Residual	18.34	10	1.83			
Lack of Fit	14.13	5	2.83	3.36	0.1049	not significant
Pure Error	4.21	5	0.84			
Cor Total	370.66	19				
Std. Dev.	1.3542		R-Squared	0.9505		
Mean	31.9397		Adj R-Squared	0.9060		
C.V.	4.2397		Pred R-Squared	0.7933		
PRESS	76.6031		Adeq Precision	14.5624		

35 °C/min, bio-oil increased rapidly with about 17.49% under 20 L/min, which is attributed to the fast heating rates cum speedy evacuation of volatiles (vapour residence time of about 10 s). Increasing heating rate above 35 °C/min under 5 L/min recorded only 8.06% increase in the oil yield due to relatively longer vapour residence time in the reactor (26 s).

Effects of heating rates, pyrolysis temperature and nitrogen flow rate on the bio-char yield is presented in Fig. 8(a–c). From Fig. 8a, there was no significant difference in the bio-char yield recorded at 20 and 50 °C/min with increasing pyrolysis temperature under constant nitrogen flow rate of 12.5 L/min. This clearly revealed that bio-char yield is governed substantially by the pyrolysis temperature. At initial temperature of 450 °C, 47.50 wt% bio-char was recorded under 20 °C/min while 50 °C/min produced 45.85 wt% bio-char at the same condition. The bio-char yield declined to 33.76 wt% when temperature increased to 750 °C at both heating rates. The slightly lower bio-char yield recorded at 50 °C/min under temperatures below 700 °C is due to rapid degradation of biomass (Mohammed et al., 2015c). Interactions between pyrolysis temperature and nitrogen flow rate under 35 °C/min (Fig. 8b) showed a continuous decline in the bio-char yield with increasing temperature in both nitrogen regimes. This suggests that impact of

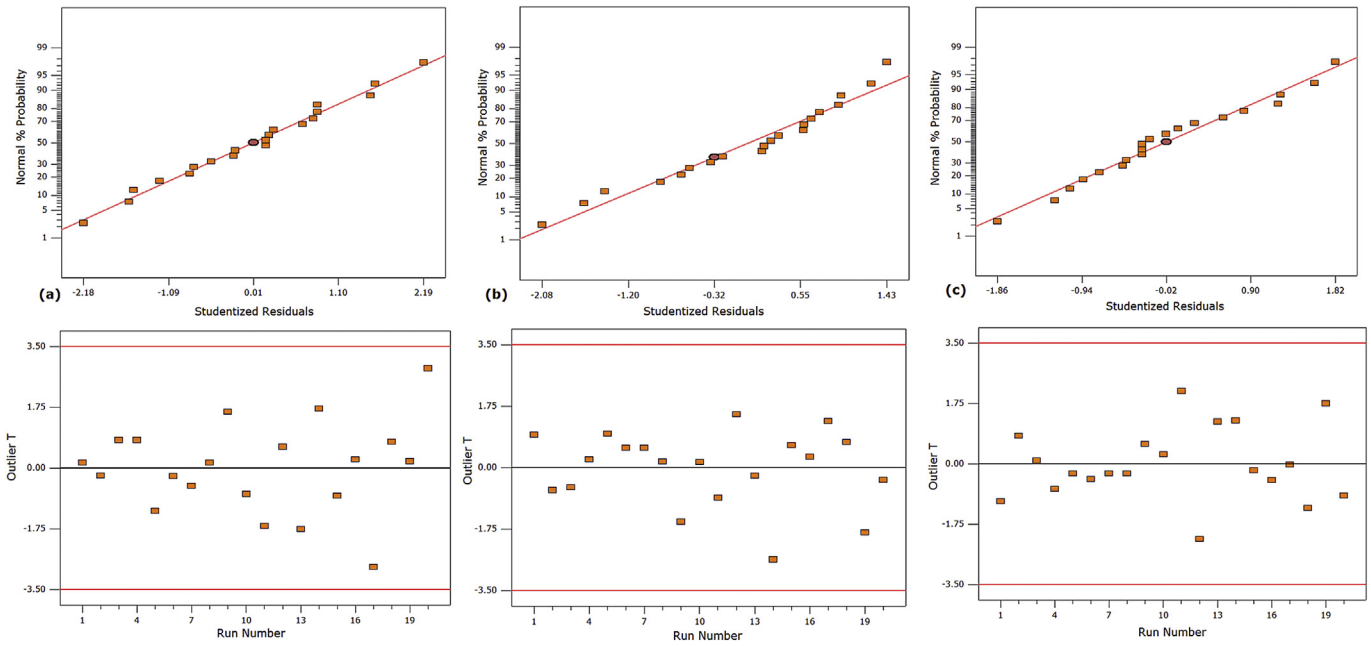

Fig. 6. Normal % probability versus studentized residuals and Outliers T versus run number. (a) bio-oil; (b) bio-char; (c) non-condensable gas.

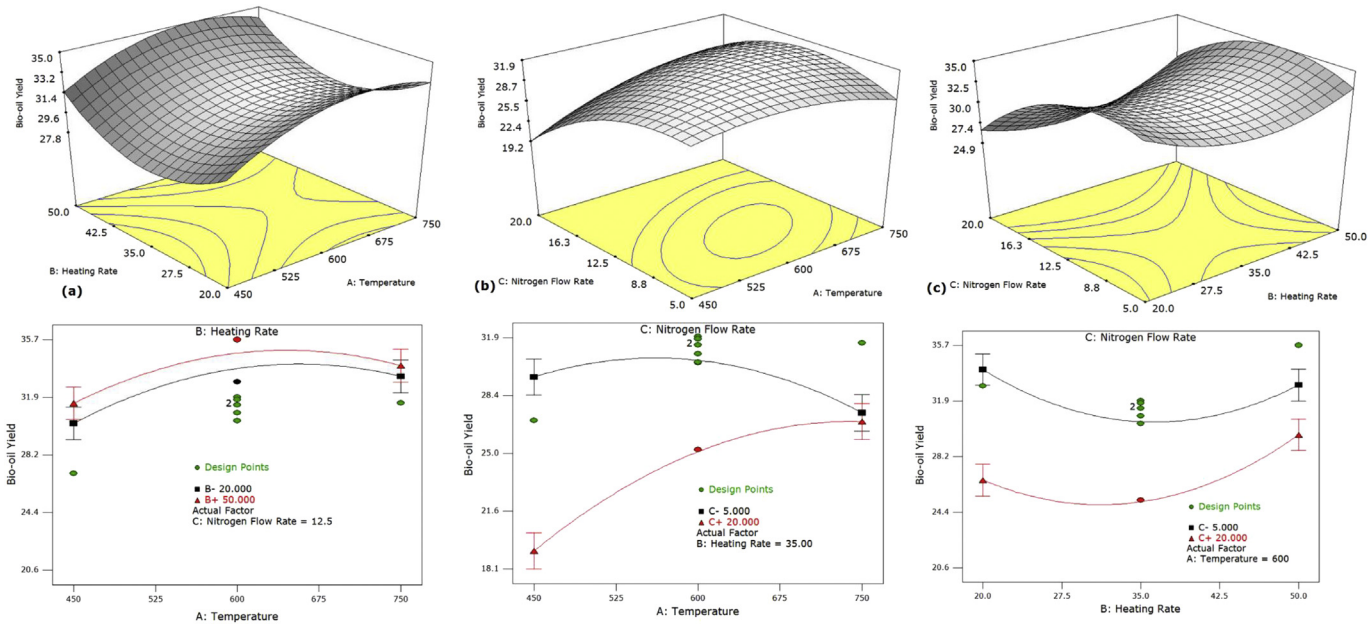

Fig. 7. 3D surface plot and corresponding interaction graphs for the combined effects of process variables on bio-oil yield. (a) Effect of heating rate and temperature at 12.5 L/min N_2; (b) Effect of nitrogen flow and temperature at 35 °C/min; (c) Effect heating rate and nitrogen flow at 600 °C.

temperature dominate the process, which is in consonant with the trend depicted by the impact of heating rate and temperature on the bio-char yield earlier observed. Further devolatilization of organic component of biomass such as dehydration of hydroxyl groups and decomposition of lignocellulose structure is said to progress with rise in pyrolysis temperature (Mohammed et al., 2015c). Interaction between heating rate and nitrogen flow on the bio-char yield at 600 °C (Fig. 8c) have no significant impact on bio-char yield. Although, less bio-char yield was recorded under 5 L/min compared to 20 L/min as the heating rate increased from 20 to 50 °C/min. This indicates that the lower bio-oil yield earlier observed under 20 L/min and heating rates (20–50 °C/min) could not be solely due to volatile less residence time in the condenser but also due to possible thermal shock brought by temperature difference between nitrogen preheating and pyrolysis reaction environments.

Impact of pyrolysis process variables on the yield of non-condensable gas are shown in Fig. 9. The combined effects of heating rate and pyrolysis temperature on the production of non-condensable gas (Fig. 9a) under 12.5 L/min nitrogen flow showed that at both 20 and 50 °C/min, the gas production increased in similar amount with increasing temperature. This signifies that production of non-condensable gas is greater affected by the pyrolysis temperature, which can be linked to secondary cracking of

volatiles and further decomposition of bio-char at higher temperatures (Yorgun and Yildiz, 2015). Non-condensable gas yield recorded at 450 °C was approximately 22.0 wt% under both heating rates but increased by nearly 50.0% when the temperature increased to 750 °C. Interaction between temperature and nitrogen flow (Fig. 9b) at 35 °C/min constant heating rate revealed that non-condensable gas yield increased with temperature at both nitrogen flow levels. As the temperature progressed from 450 to 600 °C, increase in the gas yield was not significant under 5 L/min nitrogen flow relative to 20 L/min, suggesting that most of the volatiles generated during the pyrolysis are effectively captured in the condenser, which eventually ended up in the bio-oil as rightly observed in the bio-oil yield section above. With increasing temperature beyond 600 °C, the gas yield increased rapidly in both nitrogen flow regimes, which can be ascribed to further thermal decomposition of pyrolysis vapour in addition to some uncondensed volatiles leaving the pyrolysis system as part of non-condensable gas, particularly at the higher flow rate. Furthermore, combined effect of heating rate and nitrogen flow rate at constant pyrolysis temperature of 600 °C displayed similar characteristic production profile for the non-condensable gas yield (Fig. 9c). As the heating rate increased from 20 to 50 °C/min, the change in the yield of non-condensable gas was insignificant at both nitrogen levels (5 and 20 L/min). The gas yield recorded was between 32.49-33.02 wt% and 32.46–33.34 wt% at 20 and 50 °C/min heating rate respectively throughout the carrier gas flow range.

3.5. Optimisation of process variables for bio-oil yield and validation of result

For maximum bio-oil production from the BGS, optimum condition was established by setting the variables in the range of experimental condition investigated in this study while minimizing bio-char and non-condensable gas yields as summarized in Table 7a. Accordingly, four (4) solutions were generated by the software as presented in Table 7b. Based on the highest desirability, solution number one (1) was selected. This implies that pyrolysis temperature, heating rate and nitrogen flow rate of approximately 600 °C, 50 °C/min and 11 L/min is adequate to produce optimum bio-oil of 35.0 wt% from the BGS. This prediction was validated by performing additional experiment in quadruplicates under the stated operating condition. The average bio-oil collected (Table 8) was 4.3% (36.49 wt%) higher than the predicated oil yield, however, the standard deviation is within 1.05. Therefore, this validation reiterated the adequacy of the developed model for bio-oil yield from the BGS.

3.6. Characteristics of BGS bio-oil, bio-char and non-condensable gas

Bio-oil produced from the BGS in this study consist of a two-phase liquid, organic and aqueous phase and was carefully separated into individual fractions. Some physicochemical analyses such as pH, density, water content, heating value and elemental composition (CHNSO) of the bio-oil collected at different temperatures were performed. Summary of the analytical results are presented in Table 9 and compared with standard characteristics of pyrolysis bio-oil outlined by the American Society for Testing and Materials (ASTM D7544-12). The pH value recorded for both phases are in the acidic range with organic phase having between 3.80 and 4.20 compared to an average of 3.20 for the aqueous phase. However, the relatively less acidic organic phase could be attributed to careful separation from the aqueous phase, which is generally polar in nature with compound such as acids, ketones, aldehydes, traces of phenols as the major component. Despite the separation of organic phase from the aqueous phase, trace of water in the range of 3.4–4.3 wt% remained in the organic phase. The water content of organic phase collected at 450 °C was 4.30 wt%, which is about 20% higher than the average water content of the oil collected at 600 and 700 °C. Though, this depends on how well the separation between the bio-oil phases was achieved (Mohammed et al., 2015d) however, the moisture level in the aqueous at 450 °C was 65.71 wt%

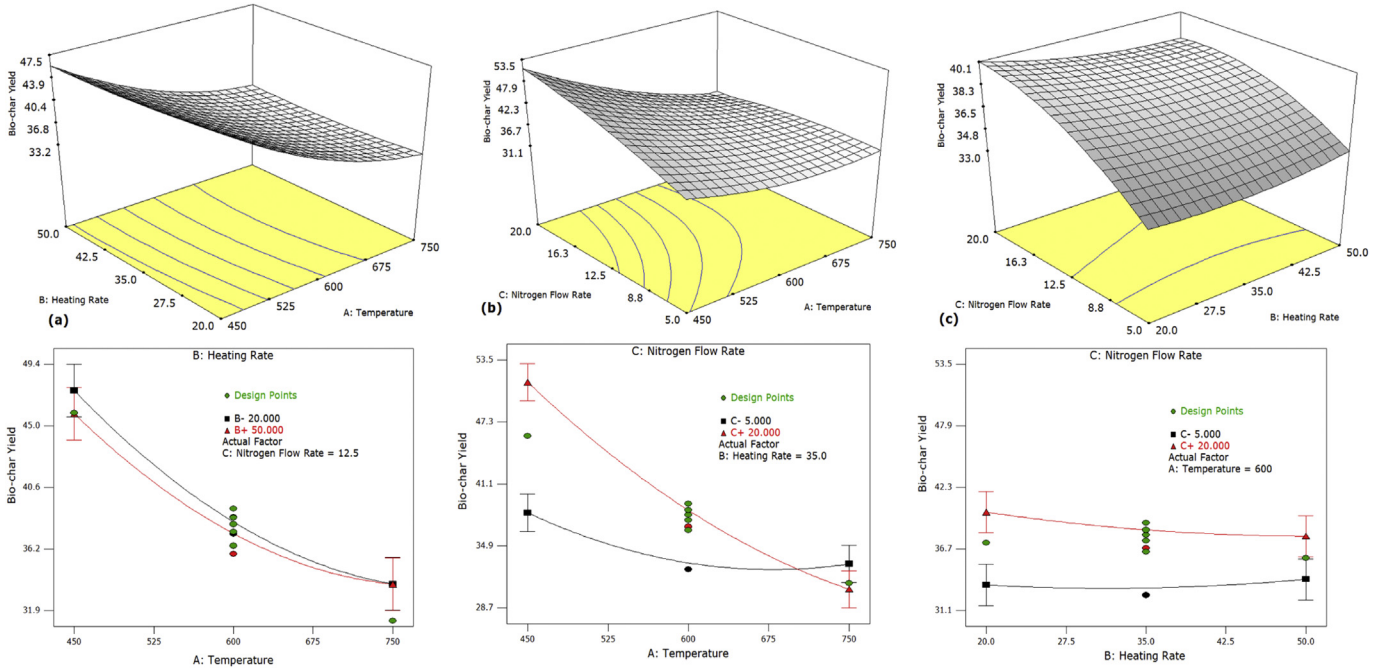

Fig. 8. 3D surface plot and corresponding interaction graphs for the combined effects of process variables on bio-char yield. (a) Effect of heating rate and temperature at 12.5 L/min N2; (b) Effect of nitrogen flow and temperature at 35 °C/min; (c) Effect heating rate and nitrogen flow at 600 °C.

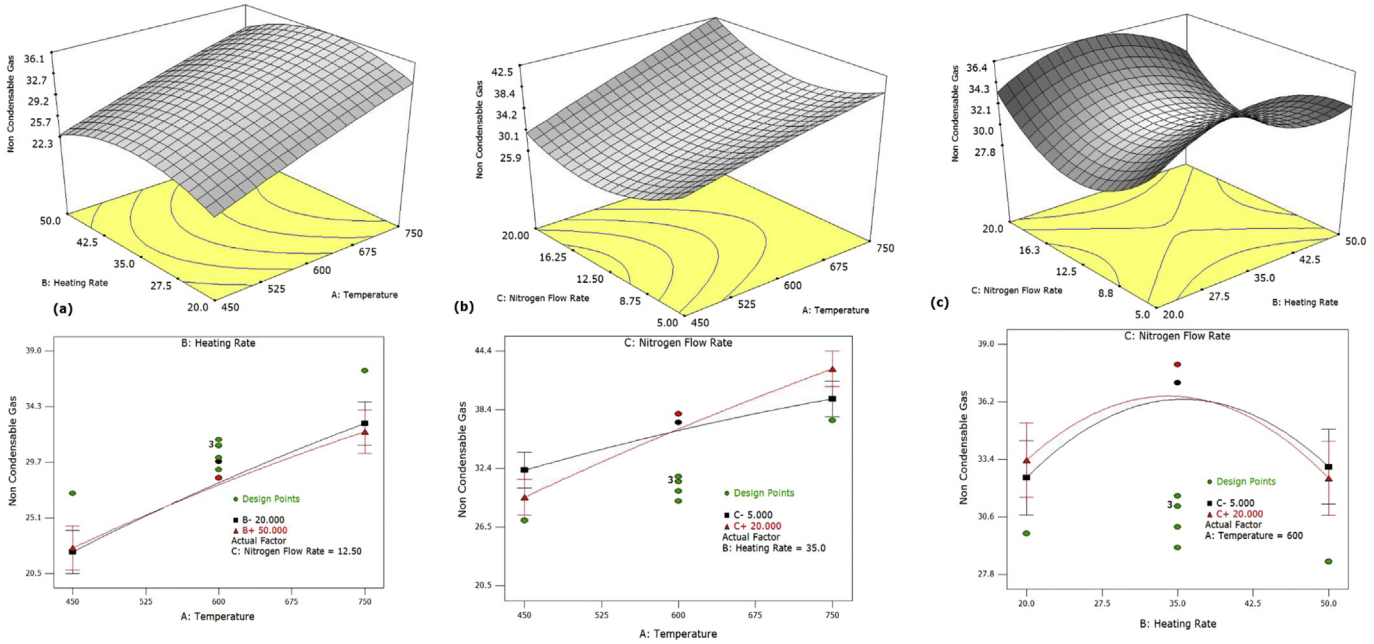

Fig. 9. 3D surface plot and corresponding interaction graphs for the combined effects of process variables on non-condensable gas yield. (a) Effect of heating rate and temperature at 12.5 L/min N2; (b) Effect of nitrogen flow and temperature at 35 °C/min; (c) Effect heating rate and nitrogen flow at 600 °C.

compared to 50.34 and 48.20 wt% water content recorded in the aqueous phase produced at 600 and 700 °C. This indicates that increasing pyrolysis temperature produce bio-oil with less water content. Literature have shown that additional thermal cracking of bio-oil, which is a typical characteristic of high pyrolysis temperature, improves chemical and vaporisation properties that in turn result in lower water content and lower molecular weight compounds (Mohammed et al., 2015c). Density of the organic phase produced at higher temperatures was approximately 8.0% lower compared to the density recorded for the bio-oil produced at 450 °C. This is an indication that bio-oil produced at 600 and 750 °C contains low molecular weight organic compounds due to possible cracking of heavy molecular weight organic compounds. Calorific values of the organic phases recorded in this study at different temperatures was approximately 24.0 MJ/kg, while carbon, hydrogen and oxygen was in the range of 43.66–49.56 wt%, 11.01–12.31 wt% and 26.97–41.01 wt% respectively. These physicochemical characteristics to a large extent, are within the ASTM specifications for both grade D and G pyrolysis oil. Characteristics of bio-oil produced at 500 °C from peanut shell reported by Zhang et al. (2011) has water content, density and calorific value of 7.8 wt%, 1.3 g/cm^3 and 21.80 MJ/kg. Similarly, Grioui et al. (2014) reported 3.1, 3.45 wt%, 1.07 g/cm^3 and 27.40 MJ/kg as pH value, water content, density and calorific value of bio-oil produced from Tunisian almond shell at 473 °C pyrolysis temperature. These properties are comparable with bio-oil characteristics recorded in this study. Physicochemical properties of bio-oil from other lignocellulosic materials are well documented in the literature. Characteristics of bio-oil from Napier grass, rice husk and sago waste was recently reported by Lim et al. (2016) and Mohammed et al. (2016c). The authors recorded carbon content in the organic phase bio-oil between 39.99 and 50.74 wt%, which is similar to the SKT-BGS organic phase bio-oil. Hydrogen content was between 6.22 and 8.43 wt%, values lower than that of BGS organic phase bio-oil. Oxygen content was in the range of 41.66–50.99 wt% while the calorific value was between 17.95 and 26.23 MJ/kg. The slight differences in the bio-oil properties from these feedstocks relative BGS bio-oil can be attributed to the disparity in structural building blocks of the individual biomass materials since the pyrolysis process conditions used are similar to the operating parameters investigated in this study.

Chemical compound in the bio-oil samples were identified using GC-MS by comparing peaks with standard spectra of compounds in the National Institute of Standards and Technology (NIST, Gaithersburg, MD, USA). Twenty most abundant chemical species were sorted using PerkinElmer TurboMass™ GC-MS software and further grouped into hydrocarbons (HC); phenols (PHOL); methyl esters (MEST); acids, aldehydes, and ketones (AAK); other value added chemicals. From Fig. 10, the component of organic phase bio-oil collected consist group of PHOL, MEST and traces of AAK and HC. These compound are products of thermal decomposition of the individual structural components (hemicellulose, cellulose and lignin) of the BGS. Generally, pyrolysis of lignocellulosic biomass proceeds through a number of chemical reactions which occur simultaneously. At temperature between 200 and 400 °C, pyrolysis proceeds via fast depolymerisation of hemicellulose and cellulose leading to the formation of anhydrosugar (levoglucosan) and unstable carbonyls and carboxylics (Collard and Blin, 2014). These compounds are polar in nature and are expected to dominate the aqueous phase bio-oil. This therefore justifies the less amount of AAK recorded in the organic phase bio-oil in this study. Similarly, under this temperature regime, carbon-carbon scission and disruption of aromatic rings occurred in lignin structure, which result in release of aldehydes, acids, alkyl-phenols and phenols (Kan et al., 2016). Consequently, PHOL recorded in the bio-oil are product of thermal decomposition of lignin. Following the composition of AAK in the organic phase, aldehyde and acid identified are benzene derived compound (Benzaldehyde, 4-methyl- and 3-Hydroxy-4-methoxybenzoic acid), which may have also originated from the lignin decomposition or a product of interaction between holocellulose and lignin derived compounds. Literature have shown that there is interaction between the different components of the biomass during pyrolysis. Studies by Hosoya et al. (2007) on cellulose-hemicellulose and cellulose-lignin

Table 7
(a) Bio-oil Optimization conditions; (b): optimised solutions. The bold values represent the selected optimised solution.

(a)

Constraints	Goal	Lower limit	Upper limit	Lower Weight	Upper Weight	Importance
Temperature	is in range	450.00	750.00	1	1	3
Heating Rate	is in range	20.00	50.00	1	1	3
Nitrogen Flow Rate	is in range	5.00	20.00	1	1	3
Bio-char Yield	minimize	31.14	53.53	1	1	3
Bio-oil Yield	maximize	20.62	35.69	1	1	5
Non Condensable Gas	minimize	25.31	38.96	1	1	3

(b)

Solution number	Temperature (°C)	Heating Rate (°C/min)	N2 Flow Rate (L/min)	Bio-char Yield (wt%)	Bio-oil Yield (wt%)	N/gas Yield (wt%)	Desirability	Remark
1	**598.81**	**50.00**	**11.09**	**37.0**	**35.0**	**28.0**	**0.8490**	**Selected**
2	595.41	50.00	10.94	37.0	35.0	28.0	0.8490	
3	616.73	50.00	11.08	36.4	35.1	28.6	0.8474	
4	582.61	20.00	9.05	37.0	34.7	28.3	0.8349	

Table 8
Bio-oil yield predicated at optimized condition and experimental value.

Experimental run	Temperature (°C)	Heating Rate (°C/min)	N2 Flow Rate (L/min)	Bio-oil Yield (wt%)	
				Predicted	experimental
1	600	50	11	35.00	36.04
2	600	50	11	35.00	35.99
3	600	50	11	35.00	37.11
4	600	50	11	35.00	36.81
Average				**35.00**	**36.49**

Table 9
Physicochemical properties of bio-oil from BGS collected at 50 °C/min, 11L/min and different temperatures.

Bio-oil Property	450 °C		600 °C		750 °C		ASTM Specification	
	Organic	Aqueous	Organic	Aqueous	Organic	Aqueous	Grade D	Grade G
pH	3.80 ± 0.01	3.20 ± 0.01	4.10 ± 0.01	3.20 ± 0.01	4.20 ± 0.01	3.10 ± 0.01	Report	Report
Water content (wt%)	4.30 ± 0.21	65.71 ± 1.01	3.44 ± 0.18	50.34 ± 1.71	3.56 ± 0.21	48.20 ± 1.88	30 max.	30 max.
Density (g/cm^3)[a]	1.00 ± 0.01	1.03 ± 0.01	0.93 ± 0.01	1.03 ± 0.01	0.92 ± 0.01	1.02 ± 0.01	1.10–1.30	1.10–1.30
LHV (MJ/Kg)	23.80 ± 0.11	13.22 ± 0.11	24.27 ± 0.11	13.89 ± 0.11	24.01 ± 0.11	14.10 ± 0.11	15.00 min.	15.00 min.
Carbon (C) (wt%)	43.66 ± 0.52	–	48.10 ± 0.51	–	49.56 ± 0.52	–	–	–
Hydrogen (H) (wt%)	12.31 ± 0.14	–	11.94 ± 0.16	–	11.01 ± 0.14	–	–	–
Nitrogen (N) (wt%)	2.01 ± 0.01	–	1.88 ± 0.01	–	1.70 ± 0.01	–	–	–
Sulphur (S) (wt%)	1.01 ± 0.01	–	0.92 ± 0.01	–	0.76 ± 0.01	–	0.05 max.	0.05 max.
Oxygen (O) (wt%)[b]	41.01 ± 0.21	–	37.16 ± 0.18	–	36.97 ± 0.20	–	–	–

Values are the means (n = 3) ± standard deviations.
[a] Determined at 20 °C.
[b] Calculated by difference [100-sum (C, H, S, N)]; max: maximum; min: minimum.

interactions in wood pyrolysis at gasification temperature showed that during cellulose-lignin pyrolysis, lignin enhanced the formation of low molecular weight products from cellulose and inhibited char formation while cellulose on the other hand deters formation of secondary char from lignin but promoted the yield of lignin-derived phenolics. They reported that there is no strong interaction between cellulose and hemicellulose during pyrolysis. Similarly, Wang et al. (2011) reported that interaction between hemicellulose and lignin during pyrolysis favours production lignin-derived phenolics but inhibits formation of hydrocarbons. Contrary to the findings by Hosoya et al. (2007), they reported that there is strong interaction between hemicellulose-cellulose which promotes the formation of furans but inhibits production of levoglucosan. They also stated that the presence of cellulose favoured the yield of hemicellulose-derived acetic acid and furfural. MEST detected in the organic phase bio-oil could be linked to thermal decomposition of pectin, a structural polysaccharide in primary cell walls of terrestrial plant (Demirbas, 2009).

Figure 10 also shows distribution of chemical compound in the organic phase bio-oil with respect to pyrolysis temperature. Increasing pyrolysis temperature from 450 to 750 °C, the amount of MEST detected in the organic phase decreased by a factor of two (2) at 600 °C and a factor of six (6) at pyrolysis temperature of 750 °C. This trend is an indication of possible thermal decomposition of heavy molecular weight MEST to produce smaller organic molecules. Similarly, the total phenolic content in the organic phase recorded at 450 °C was 74.08%, which increased to 77.20% at 600 °C and 82.28% at 750 °C, suggesting higher pyrolysis temperature promotes release of phenols from the lignin component of the biomass. This observation is in good agreement with the report of Demirbas (2009). The author observed that primary degradation of lignin generates maximum phenolics such as syringols and guaiacols at temperature between 477 and 527 °C while secondary decomposition of lignin promotes phenol production with

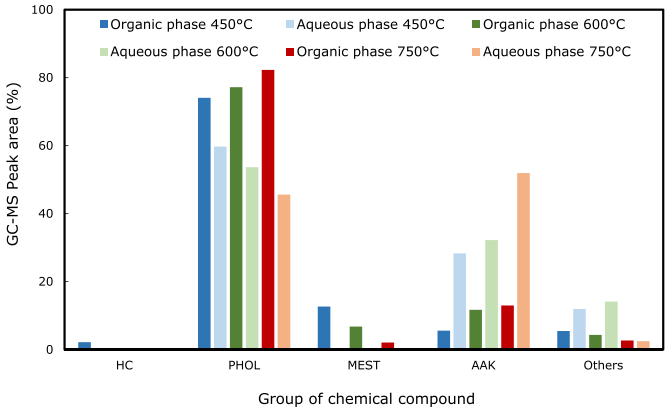

Fig. 10. Group of chemical compounds detected in the SKT-BGS bio-oil at different pyrolysis temperature. (HC) hydrocarbon; (PHOL) phenol; (MEST) methyl esters; (AAK) acid, aldehydes and ketones.

increasing temperature. On the other hand, the composition of AAK in the organic phase increased with increasing pyrolysis temperature. This could be attributed to polymerization of active short-chain organic molecules generated from MEST and other long-chain molecules with the unstable carbonyls and carboxylics during pyrolysis vapour condensation. PHOL, which constituted the largest proportion in the organic phase can be transformed into fuel and other valuable products. The chemical compound detected in the aqueous phase bio-oil (Fig. 10) were mainly AAK, PHOL and other value added polar chemical compound. The value added chemicals identified are mostly levoglucosan (sugars), a product of holocellulose decomposition and nitrogen containing oxygenates such as imidazole. Bio-oil aqueous phase is generally considered less important and often discarded as pyrolysis by-products due to lack of specific applications. However, recent studies have proposed production of hydrogen via catalytic aqueous, and steam reforming processes from this stream (Resende et al., 2015). Yet, these processes require complex system, which calls for further studies in order to understand the reaction mechanisms. Imidazole is an important material in polymer industry. There has been growing interest in the synthesis and application of imidazole based polymer, N-vinylimidazole. This is because homo- and copolymers of N-vinylimidazole belong to a rapidly emerging class of polymeric materials. Beletskaya et al. (2010) employed N-vinylimidazole for catalyzing Michael addition of uracil, 1H-1,2,4-triazole, succinimide, 3,5-dimethyl-1H-1,2,4-triazole, and oxazolidin-2-one to methyl acrylate, but-3-en-2-one, cyclohex-2-en-1-one, and methyl vinyl sulfone. This is interesting, considering the minimal energy requirement for the reaction conducted in water at room temperature. Poly (N-vinylimidazole also serves as indicator in chemical reactions that produce oxygen, which explains its usefulness as biosensors for phenolic compounds, and biomarkers for biomass smoke exposure. Metal ion binding properties of imidazole and poly (1-vinylimidazole) have been reported by Takafuji et al. (2004). Furthermore, conversion of water soluble renewable organic materials has been characterised with high conversion efficiency. Studies by Timko et al. (2006) on conversion and selectivity of a Diels-Alder cycloaddition by use of emulsions of carbon dioxide and water revealed that the reaction in emulsions of water and carbon dioxide leads to the high selectivity and conversion that are characteristic of water. Consequently, aqueous phase from the pyrolysis of BGS represent environmentally benign stream that can be used for production of valuable chemicals.

Non-condensable gas produced at the optimum pyrolysis condition was analysed offline. The gas was collected in SKC polypropylene fitted gas sampling bag and analysed following the protocol outlined in Mohammed et al. (2017). Methane (8.95%), hydrogen (4.02%), carbon monoxide (20.19%) and carbon dioxide (28.44%) were detected, which can be attributed to carbon-carbon scission within the biomass structural components and demethylation of final pyrolysis residue. High proportion of carbon monoxide and carbon dioxide in the gas could be ascribed to the catalytic effect of the mineral elements identified in the ash. Potassium (K) was identified as the major components of the BGS constituting approximately 73 wt% of the total ash (Table 2). Wang et al. (2010) evaluated catalytic effects of potassium carbonate and calcium hydroxide during pyrolysis of pine wood in a fixed-bed reactor. The authors reported that catalytic activity of potassium promoted overall production Hydrogen, carbon monoxide and carbon dioxide. BGS pyrolysis non-condensable gas could be used to provide additional to the pyrolysis system via combustion. The stream could be recycled to the pyrolysis system to enrich the hydrogen/carbon monoxide ratio, a requirement for production of liquid fuel from synthesis gas through Fischer-Tropsch (FT) synthesis.

BGS bio-char collected at different pyrolysis temperature (450, 600 and 750 °C) were analysed for proximate and ultimate properties as summarised in Table 10. From the result of proximate analysis, ash content of the bio-char produced at 450 °C was 16.12 wt%. This value increased by 14% and 22% when the pyrolysis temperature was 600 and 750 °C due to the increased devolatilization with temperature during the pyrolysis. This also explains the decline trend of remnant volatile component in the bio-char with pyrolysis temperature. The fixed carbon in the bio-char was between 60.30 and 68.28 wt%, suggesting BGS bio-char is highly carbonaceous. Calorific value (HHV) of produced bio-char decreased with increasing pyrolysis temperature, owing to the release of more volatile matter with temperature and the resulting solid constituted large portion of non-combustible material (Mohammed et al., 2014). From the ultimate analysis result, O/C

Table 10
Characteristics of BGS bio-char produced at different pyrolysis temperature.

Properties	Pyrolysis temperature (°C)		
	450	600	750
Proximate analysis (wt% db.)			
Ash content	16.12 ± 0.40	18.34 ± 0.43	19.66 ± 0.41
Volatile matter	23.58 ± 0.21	16.92 ± 0.23	12.06 ± 0.16
Fixed carbon	60.30 ± 2.04	64.74 ± 2.11	68.28 ± 2.41
FC/[VM + FC]	0.72	0.79	0.85
HHV (MJ/kg)	28.78 ± 0.11	26.11 ± 0.11	24.98 ± 0.11
Ultimate analysis (wt% db.)			
Carbon	62.22 ± 1.77	74.15 ± 1.78	81.02 ± 1.80
Hydrogen	5.08 ± 0.13	3.78 ± 0.11	2.96 ± 0.10
Nitrogen	0.76 ± 0.03	0.58 ± 0.03	0.36 ± 0.03
Sulphur	0.66 ± 0.03	0.42 ± 0.03	0.26 ± 0.03
Oxygen*	31.28 ± 0.93	21.07 ± 0.93	15.4 ± 0.90
O/C (mole ratio)	0.38	0.21	0.14
Physisorption analysis			
BET(m^2/g)	0.07 ± 0.02	1.92 ± 0.02	6.01 ± 0.02
Pore volume (cm^3/g)	0.019 ± 0.00	0.15 ± 0.00	0.30 ± 0.00
EDX mineral analysis (wt%)			
Magnesium	0 ± 0.00	1.51 ± 0.04	1.56 ± 0.04
Aluminum	1.83 ± 0.03	2.11 ± 00	5.46 ± 00
Silica	4.33 ± 0.18	10.03 ± 0.24	10.86 ± 0.24
Phosphorus	5.50 ± 0.12	1.28 ± 0.02	1.56 ± 0.02
Sulphur	7.33 ± 0.19	1.14 ± 0.01	1.56 ± 0.01
Chlorine	3.50 ± 0.15	2.52 ± 0.02	3.83 ± 0.02
Potassium	68.33 ± 1.43	78.57 ± 1.54	72.11 ± 1.54
Calcium	1.83 ± 0.06	1.28 ± 0.04	3.05 ± 0.18
Iron	1.33 ± 0.01	1.56 ± 0.01	ND

Values are the means (n = 3) ±standard deviation. (VM): volatile matter; (FC): fixed carbon; (HHV): higher heating value; (C) carbon; (O): oxygen.

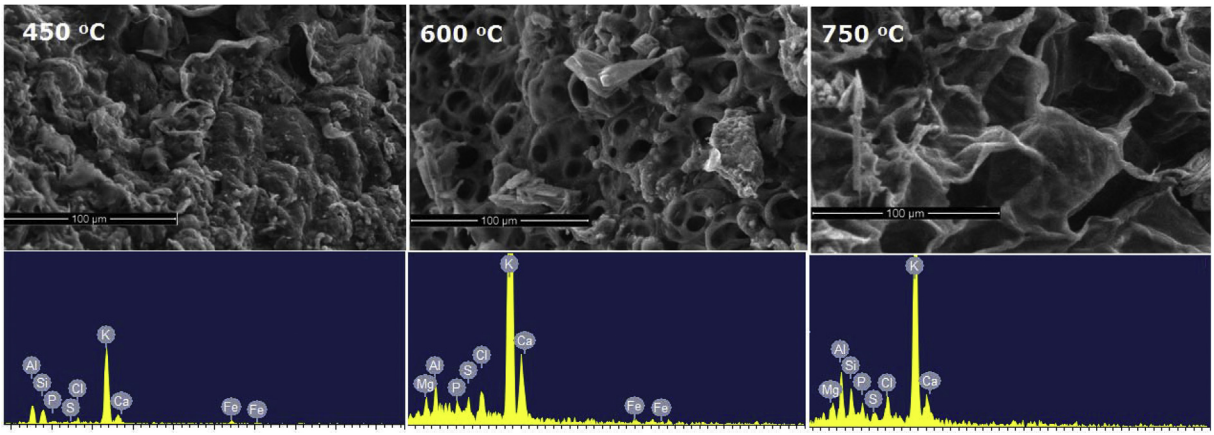

Fig. 11. SEM-EDX of SKT-BGS bio-char at different pyrolysis temperature.

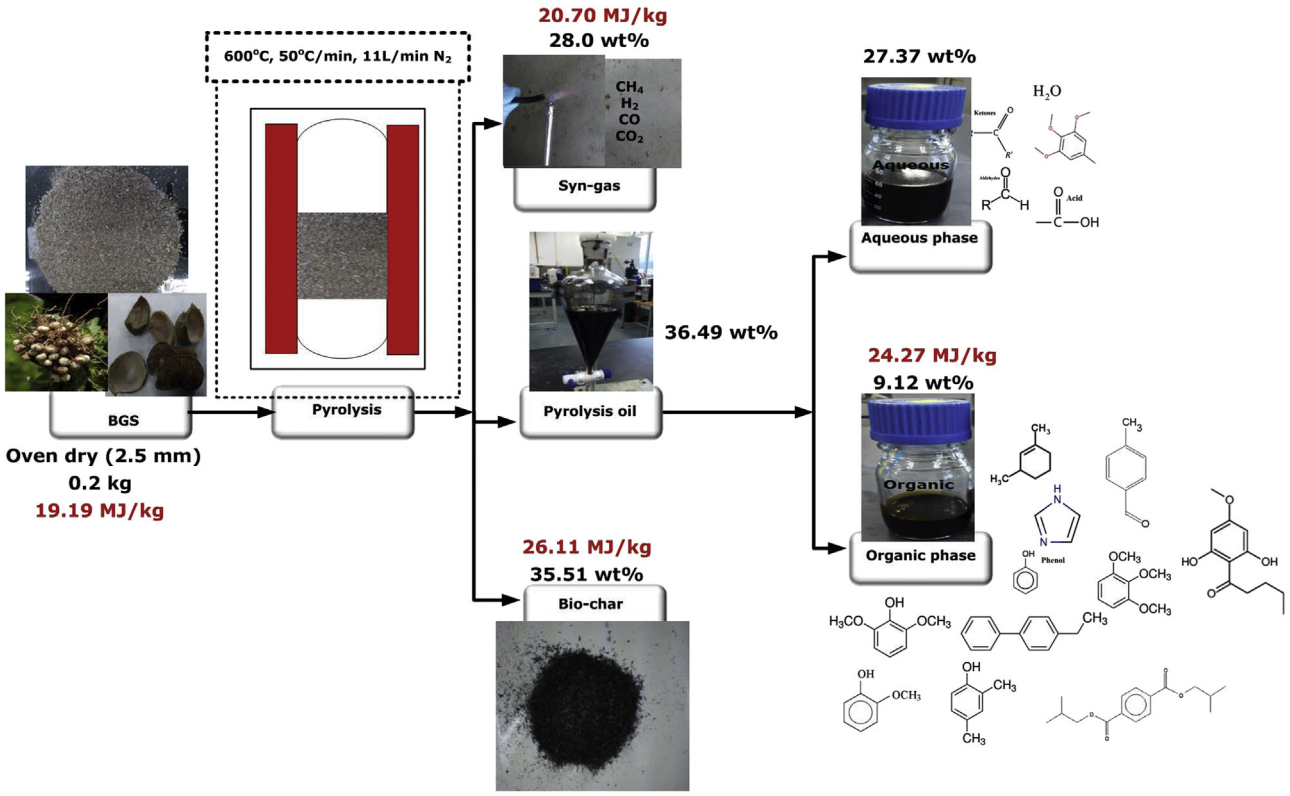

Fig. 12. Mass and energy flow of BGS pyrolysis in a fixed bed reactor.

molar ratio of the produced char increased with increasing pyrolysis temperature, indicating increased bio-char stability. Literature have shown that O/C molar ratio of bio-char below 0.2 connotes half-life of about 1000years (Mohammed et al., 2017). The SEM-EDX result (Fig. 11) indicates porous structures in the produced bio-char with higher pyrolysis temperature resulting in formation larger pores. This observation was further evaluated with physisorption analyser. The pore size of the bio-char produced at 450 °C was 0.019 cm^3/g (Table 10), which became approximately eight (8) and sixteen (16) times larger in the bio-char collected at 600 and 750 °C. Similarly, the specific surface areas of the bio-chars produced at higher temperatures were between 27 and 86 times larger relative to the specific surface area recorded for bio-char at 450 °C. The improved pore and surface characteristics of the bio-char with temperature is attributed to high level of devolatilization recorded with increasing pyrolysis temperature. The characteristics of BGS bio-char recorded in this study, particularly at 600 °C, is similar to the SKT-BGS bio-char properties obtained at 600 °C reported in the literature (Mohammed et al., 2016a). EDX results (Fig. 11) reveal spectra of some minerals (K, Ca, Mg and P), which are important nutrient for agricultural crops production.

3.7. Energy analysis of BGS pyrolysis process

Energy yield of pyrolysis products is obtained from mass flow and higher heating values of the organic phase bio-oil, bio-char and non-condensable gas with respect to that of the feedstock. Fig. 12 shows the mass flow collected at optimised condition and the

corresponding heating values of each stream. The energy yield of the organic phase bio-oil was about 16% compared to 48% and 30% recorded for the bio-char and non-condensable gas. This is attributed to lower mass production of the organic phase. Higher energy yield from the bio-char is not surprising due to the stream high mass flow, which is 27% higher than the mass flow of the non-condensable gas and approximately four-folds the mass flow of organic phase. The energy distribution from the pyrolysis of BGS recorded in this study is similar to energy distribution of pyrolysis products obtained from the pyrolysis of poplar wood in a fixed bed reactor at 600 °C and 50 °C/min reported by Chen et al. (2016). The authors showed that energy yield from bio-char was 46.69% while bio-oil and non-condensable gas had 31.84% and 22.34% energy yield. They attributed the higher energy yield recorded from the bio-char to higher heating value (32.10 MJ/kg) despite the lower mass yield while the relatively lower energy yield from the bio-oil was ascribed to lower calorific value (13.93 MJ/kg) in spite of the higher mass yield (41.67 wt%). Although, the authors did not state the portion of the bio-oil used in the energy analysis.

Energy consumption in the pyrolysis process can be related to the overall energy yield of the pyrolysis products, which can be used as an indicator of pyrolysis process energy efficiency. In this study, the total energy input such as energy consumption during pre-processing (drying and grinding) and pyrolysis stage (pyrolysis reactor and cooling) is summarized in Table 11. BGS was bone dried in an electrical oven for 12 h. For 1.0 kg bone dried biomass processing, 1 h chiller and pyrolysis reactor operation, the total electrical energy consumption was 82.67 MJ (22.96 kWh). The ratio of energy output to energy input recorded is 0.21. This indicates that the total energy produced from the process is far less than the energy input. The highest contributor to the energy consumption is the drying stage, consuming approximately 84% of the total energy input. Pyrolysis stage, which is the heart of the process consumed only about 15.4% of the total energy consumption. This mean that the energy efficiency of the process can be improved by reducing the energy consumption at drying stage. Ning et al. (2013) stated that the challenge of high energy requirement of pyrolysis system may be compensated through efficient utilization of other pyrolysis products such as bio-char and non-condensable gas. They recorded about 81% higher energy efficiency when energy from bio-char combustion was integrated into the system. Studies by Nizami et al. (2017) on waste-based biorefinery showed that pyrolysis process as one of the waste to energy technologies had the lowest efficiency (17%) compared to other technologies such as anaerobic digestion, transesterification and refuse derived fuel with corresponding efficiency in the range of 25–30%, 33–38% and 18–30%. Despite this, the pyrolysis technology electricity generation potential as determined by the authors was 2–3folds higher relative to that of the other technologies, which makes it a more viable option for conversion of waste to energy. Combustion of bio-char and non-condensable gas can generate steam and hot air, which could be used for drying the biomass. This would definitely reduce the energy requirement significantly and make the process more energy efficient.

Table 11
Energy evaluation of BGS pyrolysis process in a fixed bed reactor.

Process Stage	Energy (MJ)		Output/input ratio
	Input	output	
Drying	69.12	–	–
Grinding	0.81	–	–
Pyrolysis reactor	5.83	–	–
cooling water	6.91	–	–
Organic bio-oil	–	2.21	–
Bio-char	–	9.27	–
Non-condensable gas	–	5.80	–
Total	**82.67**	**17.28**	**0.21**

3.8. Future outlook

Valorisation of waste from food crops or agro-wastes such as Bambara groundnut shell via pyrolysis present a sustainable approach for bioenergy production. Bio-oil from Bambara groundnut shell has high calorific value, which can be upgraded into high-grade biofuel. Catalytic upgrading of the bio-oil and techno-economic analysis of the process need further understanding.

4. Conclusions

The decomposition behaviour and kinetic parameters of Bambara groundnut shell was investigated. The degradation proceeded in three different stages. Stage I was attributed to removal moisture while stages II and III represent the main pyrolysis process. The kinetics was evaluated with single-step global model. The SSGM model was found to a large extent to be appropriate for modelling the decomposition profile of BGS and reasonably predicted the kinetic parameters of the sample. Intermediate pyrolysis of BGS was conducted in a fixed bed reactor. Effect of pyrolysis temperature (450–750 °C), heating rate (20–50 °C/min) and nitrogen flow rate (5–25 L/min) were investigated collectively. Optimum bio-oil yield of 36.49 wt% was recorded at 600 °C, 50 °C/min and 11 L/min, which is about 11.28% higher than the bio-oil yield from SKT-BGS reported in the literature under the same pyrolysis temperature. The bio-oil collected was comprehensively characterised. The result of analysis revealed that BGS bio-oil constitutes predominantly phenolics, trace of fatty acid methyl esters and hydrocarbon. These compounds are important feedstock for production of quality biofuel and valuable chemicals. Characteristics of bio-char indicates that is can be applied in adsorption processes or as biofertilizer or solid fuel. This study revealed Bambara groundnut shell, a residue from food crop, is a good material for sustainable bioenergy production.

Acknowledgment

The project was supported by the Crops for the Future (CFF) and University of Nottingham under the grant BioP1-005.

References

Beletskaya, I.P., Tarasenko, E.A., Khokhlov, A.R., Tyurin, V.S., 2010. Poly (N-vinylimidazole) as an efficient and recyclable catalyst of the Aza-Michael reaction in water. Russ. J. Org. Chem. 46 (4), 461–467.
Biswas, K.K., Umeki, K., Yang, W., Blasiak, W., 2011. Change of pyrolysis characteristics and structure of woody biomass due to steam explosion pre-treatment. Fuel Process. Technol. 92, 1849–1854.
Brough, S.H., Azam-Ali, S.N., 1992. The effect of soil moisture on the proximate composition of Bambara groundnut (Vigna subterranea (L) Verdc). J. Sci. Food Agric. 60 (2), 197–203.
Chen, D., Li, Y., Cen, K., Luo, M., Li, H., Lu, B., 2016. Pyrolysis polygeneration of poplar wood: effect of heating rate and pyrolysis temperature. Bioresour. Technol. 218, 780–788.
Collard, F.X., Blin, J., 2014. A review on pyrolysis of biomass constituents: mechanisms and composition of the products obtained from the conversion of cellulose, hemicelluloses and lignin. Renew. Sustain. Energy Rev. 38, 594–608.
Demirbas, A., 2009. Fuel properties of pyrolysis oils from biomass. Energy Sources Part A Recovery, Util. Environ. Eff. 31, 412–419.
Grioui, N., Halouani, K., Agblevor, F.A., 2014. Bio-oil from pyrolysis of Tunisian almond shell: comparative study and investigation of aging effect during long storage. Energy Sustain. Dev. 21, 100–112.
Hosoya, T., Kawamoto, H., Saka, S., 2007. Cellulose-hemicellulose and cellulose-lignin interactions in wood pyrolysis at gasification temperature. J. Anal. Appl. Pyrolysis 80, 118–125.

Imam, T., Capareda, S., 2012. Characterization of bio-oil, syn-gas and bio-char from switchgrass pyrolysis at various temperatures. J. Anal. Appl. Pyrolysis 93, 170–177.
International Energy Outlook (IEO) 2016. http://www.eia.gov/forecasts/ieo/pdf/0484(2016).pdf, (Access 15 October 2016).
Kan, T., Strezov, V., Evans, T.J., 2016. Lignocellulosic biomass pyrolysis: a review of product properties and effects of pyrolysis parameters. Renew. Sustain. Energy Rev. 57, 1126–1140.
Kishinevsky, B.D., Zur, M., Friedman, Y., Meromi, G., Ben-Moshe, E., Nemas, C., 1996. Variation in nitrogen fixation and yield in landraces of Bambara groundnut (*Vigna subterranea* L.). Field Crops Res. 48 (1), 57–64.
Kuprianov, V.I., Arromdee, P., 2013. Combustion of peanut and tamarind shells in a conical fluidized-bed combustor: a comparative study. Bioresour. Technol. 140, 199–210.
Lesnikovich, A., Levchik, S.A., 1983. Method of finding invariant values of kinetic parameters. J. Therm. Anal. Calorim. 27, 89–93.
Lim, C.H., Mohammed, I.Y., Abakr, Y.A., Kazi, F.K., Yusup, S., Lam, H.L., 2016. Novel input-output prediction approach for biomass pyrolysis. J. Clean. Prod. 136, 51–61.
Mohale, K.C., Belane, A.K., Dakora, F.D., 2014. Symbiotic N nutrition, C assimilation, and plant water use efficiency in Bambara groundnut (Vigna subterranea L. Verdc) grown in farmers' fields in South Africa, measured using 15N and 13C natural abundance. Biol. Fertil. Soils 50 (2), 307–319.
Mohammed, I.Y., Abakr, Y.A., Musa, M., Yusup, S., Singh, A., Kazi, F.K., 2016a. Valorization of Bambara groundnut shell via intermediate pyrolysis: products distribution and characterization. J. Clean. Prod. 139, 717–728.
Mohammed, I.Y., Abakr, Y.A., Yusup, S., Kazi, F.K., 2017. Valorization of Napier grass via intermediate pyrolysis: optimization using response surface methodology and pyrolysis products characterization. J. Clean. Prod. 142, 1848–1866.
Mohammed, I.Y., Kazi, F.K., Abakr, Y.A., Yusuf, S., Razzaque, M.A., 2015d. Novel method for the determination of water content and higher heating value of pyrolysis oil. BioResources 10 (2), 2681–2690.
Mohammed, I.Y., Abakr, Y.A., Kabir, F., Yusup, S., 2015b. Effect of aqueous pretreatment on pyrolysis characteristics of Napier grass. J. Eng. Sci. Technol. 10 (11), 1487–1496.
Mohammed, I.Y., Abakr, Y.A., Kazi, F.K., Yusuf, S., Alshareef, I., Chin, S.A., 2015c. Pyrolysis of Napier grass in a fixed bed reactor: effect of operating conditions on product yields and characteristics. BioResources 10 (4), 6457–6478.
Mohammed, I.Y., Abakr, Y.A., Kazi, F.K., Yusup, S., 2016b. Effects of pre-treatments of Napier grass with deionized water, sulfuric acid and sodium hydroxide on pyrolysis oil characteristics. Waste Biomass Valorization 1–9. http://dx.doi.org/10.1007/s12649-016-9594-1.
Mohammed, I.Y., Abakr, Y.A., Kazi, F.K., Yusup, S., Alshareef, I., Chin, S.A., 2015a. Comprehensive characterization of Napier grass as a feedstock for thermochemical conversion. Energies 8 (5), 3403–3417.
Mohammed, I.Y., Kazi, F.K., Yusuf, S.B., Alshareef, I., Chin, S.A., 2014. Higher heating values (HHV) prediction model from biomass proximate analysis data. In: International Conference & Exhibition on Clean Energy October 20–22, Quebec, Canada.
Mohammed, I.Y., Lim, C.H., Kazi, F.K., Yusup, S., Lam, H.L., Abakr, Y.A., 2016c. Co-pyrolysis of rice husk with underutilized biomass species: a sustainable route for production of precursors for fuels and valuable chemicals. Waste Biomass Valorization 1–11. http://dx.doi.org/10.1007/s12649-016-9599-9.
Muradov, N., Fidalgo, V., Gujar, N., Garceau, A., T-Raissi, A., 2012. Production and characterization of Lemna minor bio-char and its catalytic application for biogas reforming. Biomass Bioenergy 42, 123–131.
Musa, M., Massawe, F., Mayes, S., Alshareef, I., Singh, A., 2016. Nitrogen Fixation and N-balance studies on Bambara Groundnut Landraces grown on tropical acidic soils of Malaysia. Commun. Soil Sci. Plant Anal. 47 (4), 533–542.
Mwale, S.S., Azam-Ali, S.N., Massawe, F.J., 2007. Growth and development of Bambara groundnut (Vigna subterranea) in response to soil moisture: 1. Dry matter and yield. Eur. J. Agron. 26 (4), 345–353.
Ning, S.-K., Hung, M.-C., Chang, Y.-H., Wan, H.-P., Lee, H.-T., Shih, R.-F., 2013. Benefit assessment of cost, energy, and environment for biomass pyrolysis oil. J. Clean. Prod. 59, 141–149.
Nizami, A.S., Shahzad, K., Rehan, M., Ouda, O.K.M., Khan, M.Z., Ismail, I.M.I., Almeelbi, T., Basahi, J.M., Demirbas, A., 2017. Developing waste biorefinery in Makkah: a way forward to convert urban waste into renewable energy. Appl. Energy 186, 189–196.
Patnaik, A.S., Goldfarb, J.L., 2015. Continuous activation energy representation of the Arrhenius equation for the pyrolysis of cellulosic materials: feed corn stover and cocoa shell biomass. Cellul. Chem. Technol. 263–270.
Resende, K.A., Ávila-Neto, C.N., Rabelo-Neto, R.C., Noronha, F.B., Hori, C.E., 2015. Thermodynamic analysis and reaction routes of steam reforming of bio-oil aqueous fraction. Renew. energy 80, 166–176.
Starink, M., 2003. The determination of activation energy from linear heating rate experiments: a comparison of the accuracy of isoconversion methods. Thermochim. Acta 404, 163–176.
Takafuji, M., Ide, S., Ihara, H., Xu, Z., 2004. Preparation of Poly (1-vinylimidazole)-grafted magnetic nanoparticles and their application for removal of metal ions. Chem. Mater. 16 (10), 1977–1983.
Timko, M.T., Allen, A.J., Danheiser, R.L., Steinfeld, J.I., Smith, K.A., Tester, J.W., 2006. Improved conversion and selectivity of a Diels-Alder cycloaddition by use of emulsions of carbon dioxide and water. Ind. Eng. Chem. Res. 45 (5), 1594–1603.
United States Census Bureau, 2016. International Data Base (USCB). https://www.census.gov/population/international/data/idb/worldpopgraph.php (Accessed 05 January 2017).
Vyazovkin, S., Burnham, A.K., Criado, J.M., Pérez-Maqueda, L.A., Popescu, C., Sbirrazzuoli, N., 2011. ICTAC Kinetics Committee recommendations for performing kinetic computations on thermal analysis data. Thermochim. Acta 520, 1–19.
Wang, S.R., Guo, X.J., Wang, K.G., Luo, Z.Y., 2011. Influence of the interaction of components on the pyrolysis behaviour of biomass. J. Anal. Appl. Pyrolysis 91, 183–189.
Wang, Z., Wang, F., Cao, J., Wang, J., 2010. Pyrolysis of pine wood in a slowly heating fixed-bed reactor: potassium carbonate versus calcium hydroxide as a catalyst. Fuel Process. Technol. 91 (8), 942–950.
Yakub, M.I., Abdalla, A.Y., Feroz, K.K., Suzana, Y., Ibraheem, A., Chin, S.A., 2015. Pyrolysis of oil palm residues in a fixed bed tubular reactor. J. Power Energy Eng. 3 (04), 185.
Yorgun, S., Yıldız, D., 2015. Slow pyrolysis of paulownia wood: effects of pyrolysis parameters on product yields and bio-oil characterization. J. Anal. Appl. Pyrolysis 114, 68–78.
Zhang, C., Zhang, R., Li, X., Li, Y., Shi, W., Ren, X., Xu, X., 2011. Bench-scale fluidized-bed fast pyrolysis of peanut shell for bio-oil production. Environ. Prog. Sustain. Energy 30, 11–18.